Asian J Biol Life Sci., 2026; 15(1):159-172.
https://ajbls.com

Research Article

Benzotriazole as Privileged Scaffold: A Molecular Docking Approach toward Breast Cancer Drug Discovery

Pornima Ramdas Tambe, Rohit Jaysing Bhor*, Mahesh Hari Kolhe, Radhika Bansi Varade, Shaikh Tarnnum Bhaiya, Akanksha Sunil Tambe

Department of Pharmaceutical Chemistry, Pravara Rural College of Pharmacy Pravaranagar, Rahata, Ahmednagar, Maharashtra, INDIA.

ABSTRACT

Introduction: Breast cancer remains one of the leading causes of cancer-related mortality worldwide, particularly in hormone receptor–positive subtypes driven by estrogen signaling. In the present study, a structure-based molecular docking approach was employed to evaluate benzotriazole derivatives as potential aromatase inhibitors. **Materials and Methods:** The crystal structure of human aromatase (PDB ID: 3EQM) was retrieved from the Protein Data Bank and prepared using standard protein optimization protocols. **Results:** Twelve benzotriazole derivatives (PT-1 to PT-12) were designed and subjected to ligand preparation, energy minimization, and docking analysis using the Schrodinger Glide module. All compounds complied with Lipinski's criteria, while PT-5 exhibited one Veber violation due to high polarity. Docking scores ranged from –6.22 to –9.90 kcal/mol, indicating favorable binding interactions with the aromatase active site. **Discussion:** Notably, PT-5 demonstrated the strongest binding affinity (–9.90 kcal/mol), forming multiple conventional hydrogen bonds with VAL369, VAL370, PRO429, MET311, and THR310, along with hydrophobic and π–interactions. PT-4 and PT-11 exhibited balanced docking performance and favorable pharmacokinetic profiles, suggesting improved drug-likeness compared to PT-5. Interaction analysis revealed that residues VAL369, VAL370, ALA306, ALA307, LEU152, PHE430, MET303, and CYS437 play crucial roles in ligand stabilization through hydrogen bonding, π–π stacking, π–sulfur, and hydrophobic interactions. **Conclusion:** The conclusion was the findings highlight benzotriazole as a promising scaffold for aromatase inhibition and support further *in vitro* and *in vivo* investigations to validate its therapeutic potential in breast cancer management.

Keywords: Benzotriazole, Molecular Docking, Anticancer Activity, Aromatase Inhibitor, PDB-3EQM.

Correspondence:
Dr. Rohit Jaysing Bhor
Department of Pharmaceutical Chemistry, Pravara Rural College of Pharmacy Pravaranagar, Rahata, Ahmednagar, Maharashtra, INDIA.
Email: rohit.bhor69@gmail.com
ORCID: 0000-0002-7979-3765

Received: 09-12-2025;
Revised: 28-01-2026;
Accepted: 18-03-2026.

INTRODUCTION

Benzotriazole is a heterocyclic scaffold in medicinal chemistry due to its advantageous pharmacological features, powerful nitrogen content, strong and rigid aromatic Structure, and adaptable substitution patterns which together enable a variety of binding interactions (Agu *et al*., 2023). The Benzotriazole core target enzymes were integrated with a variety of bioactive compounds, showing potential use in the development of a scaffold design for Aromatase inhibitors (Arvindekar *et al*., 2024). Breast cancer remains one of the most prevalent malignancies and a leading cause of cancer-related mortality among women worldwide (Augusto *et al*., 2018). Hormone receptor–positive breast cancer accounts for a substantial proportion of diagnosed cases, where tumor progression is primarily driven by estrogen signaling. Estrogen plays a critical role in promoting cell proliferation and survival in breast tissue, and its biosynthesis is catalyzed by the enzyme aromatase (cytochrome P450 19A1, CYP19A1). Aromatase converts androgens such as androstenedione and testosterone into estrogens through a multi-step oxidative process (Bhatia & Thareja, 2025). Due to its central role in estrogen production, aromatase has become a well-validated therapeutic target in the treatment of postmenopausal hormone-dependent breast cancer. Aromatase inhibitors (AIs), including non-steroidal and steroidal agents, have significantly improved clinical outcomes in estrogen receptor–positive breast cancer. However, long-term therapy is often associated with adverse effects, drug resistance, and reduced therapeutic responsiveness (Briguglio *et al*., 2015). These limitations highlight the need for the discovery and development of novel scaffolds with improved efficacy, selectivity, and pharmacokinetic profiles (Du *et al*., 2016). Benzotriazole is a nitrogen-rich heterocyclic scaffold widely recognized in medicinal chemistry for its structural versatility and diverse biological activities. The benzotriazole nucleus contains three nitrogen atoms capable of forming strong hydrogen bonds

DOI: 10.5530/ajbls.20260129

Copyright Information :
Copyright Author (s) 2026 Distributed under Creative Commons CC-BY 4.0

Publishing Partner : Manuscript Technomedia. [www.mstechnomedia.com]

and electrostatic interactions, while its planar aromatic system facilitates π–π stacking and hydrophobic interactions within protein binding pockets. These structural features make Benzotriazole an attractive pharmacophore for designing enzyme inhibitors, including anticancer agents (Eissa & Gohar, 2023). Advances in computational drug discovery have accelerated the identification of promising lead compounds through structure-based approaches. Molecular docking is a powerful *in silico* technique that predicts the binding orientation, interaction pattern, and affinity of small molecules within the active site of target proteins. By analyzing protein–ligand interactions at the atomic level, docking studies provide valuable insights into binding mechanisms and support rational drug design strategies (Freihat *et al*., 2025). In the present study, a series of Benzotriazole derivatives were designed and evaluated for their inhibitory potential against aromatase using molecular docking analysis (Gadakh *et al*., 2025). The crystal structure of human aromatase (PDB ID: 3EQM) was utilized to investigate binding interactions, docking scores, and active-site complementarity (Gumede *et al*., 2025). In addition, physicochemical properties, drug-likeness parameters, and ADME characteristics were assessed to identify compounds with optimal pharmacokinetic profiles (Kifle *et al*., 2021). This integrated computational approach aims to identify promising Benzotriazole-based lead candidates for further experimental validation in breast cancer therapy (Lee *et al*., 2025).

MATERIALS AND METHODS

Target Proteins Selection

The enzyme aromatase (CYP19A1), a crucial regulator of estrogen production and a clinically proven target for hormone-dependent breast cancer, was chosen for molecular docking explorations (Lewis-Wambi & Jordan, 2009). The three-dimensional crystal structure of human aromatase complexed with an inhibitor (PDB ID: 3EQM) was provided in Figure 1 by the RCSB Protein Data Bank with https://www.rcsb.org/structure/3EQM.

Protein Preparation

For the preparation of protein, the Schrodinger Suite's Protein Preparation Wizard (Maestro, Version 2022-4) was used. crystallographic water molecules more than 5 Å from the active site were eliminated, and critical residues were kept (Li *et al*., 2020). Protonation states were optimized at physiological pH (7.0 ± 0.2) after Bond orders were assigned, and the addition of missing hydrogen atoms was done.

Preparation of ligand

Benzotriazole and its substituted scaffolds were used as ligands for the docking study in Table 1. For chemical structures, Chem Draw was used to sketch, which were then converted into three-dimensional structures (Ma & Yu, 2006). Ligands were prepared by using Schrodinger's Lig Prep module. The ligands' overall energy-minimized Potential of stereoisomers were kept, and the refined ligands were stored in Maestro format (Mardale *et al*., 2026).

RESULTS

Comparative Analysis of Physicochemical and Drug-Likeness Properties of PT-1 to PT-12

The physicochemical and drug-likeness properties of the designed molecules (PT-1 to PT-12) were evaluated in Table 2 by using key parameters including rotatable bonds, Hydrogen Bond Acceptors (HBA), Hydrogen Bond Donors (HBD), consensus LogP, Lipinski's rule of five violations, Veber rule violations, and synthetic accessibility scores. All compounds exhibited an acceptable number of rotatable bonds (3–7), indicating suitable molecular flexibility for oral bioavailability. Most molecules contained 3–5 HBAs and 0–2 HBDs, which fall within the recommended range for optimal membrane permeability and hydrogen bonding interactions with biological targets. Notably, PT-5 showed a comparatively higher number of Hydrogen Bond Donors (HBD = 5) and Acceptors (HBA = 8), which may negatively influence permeability. The consensus LogP values ranged from −0.88 to 3.75, suggesting moderate lipophilicity across the series. Compounds such as PT-3, PT-8, and PT-10 demonstrated higher LogP values (>3), indicating enhanced lipophilicity that may favor membrane penetration, while PT-5, with a negative LogP value, appeared relatively hydrophilic. Importantly, all molecules complied with Lipinski's rule of five, indicating favorable oral drug-like characteristics. With respect to molecular flexibility and polar surface considerations, all compounds except PT-5 satisfied the Veber rule, further supporting their potential oral bioavailability. The single Veber violation observed in PT-5 can be attributed to its higher hydrogen bonding capacity. The synthetic accessibility scores for the compounds ranged between 2.55 and 3.04 for most molecules, suggesting that they are relatively easy to synthesize. However, PT-5 exhibited a higher synthetic accessibility score (4.14), indicating comparatively greater synthetic complexity. The comparative evaluation reveals that PT-1, PT-2, PT-3, PT-4, PT-6, PT-8, PT-9, PT-10, PT-11, and PT-12 possess balanced physicochemical properties with good drug-likeness, no Lipinski violations, no Veber violations, and favorable synthetic accessibility. In contrast, PT-5 showed comparatively less favorable characteristics due to its higher hydrogen bonding capacity, Veber rule violation, and increased synthetic complexity. These findings suggest that the majority of the studied compounds are promising candidates for further pharmacological evaluation.

Comparative Evaluation of ADME and Pharmacokinetic Properties of PT-1 to PT-12

The ADME and pharmacokinetic profiles of the designed molecules (PT-1 to PT-12) were assessed in Table 3 by using Gastrointestinal (GI) absorption, Blood–Brain Barrier (BBB)

permeability, Cytochrome P450 (CYP) enzyme inhibition, skin permeation coefficient (Log Kp), and bioavailability score as key indicators of drug-likeness and *in vivo* performance. All compounds except PT-5 exhibited high GI absorption, indicating favorable oral absorption characteristics. The reduced GI absorption observed for PT-5 may be attributed to its higher polarity and lower lipophilicity, consistent with its poor membrane permeability. With respect to BBB permeability, the majority of the molecules (PT-1, PT-2, PT-3, PT-4, PT-6, PT-8, PT-10, and PT-11) were predicted to be BBB permeant, suggesting potential applicability in Central Nervous System (CNS)-related indications. In contrast, PT-5, PT-7, PT-9, and PT-12 were predicted to be non-BBB permeant, indicating reduced CNS exposure and potentially lower risk of central side effects for peripheral therapeutic applications. Cytochrome P450 inhibition profiling revealed notable differences among the compounds. Several molecules, including PT-2, PT-3, PT-8, and PT-10, were predicted to inhibit CYP1A2, CYP2C19, and CYP2C9, suggesting a higher likelihood of metabolic interactions. In contrast, PT-1, PT-5, and PT-7 showed no inhibitory activity against any of the

Table 1: Benzotriazole Derivatives from PT-1 to PT-12.

Code	Structure	Code	Structure
PT-1	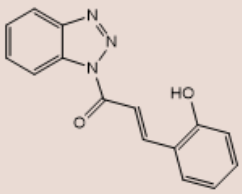	PT-7	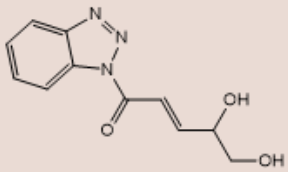
PT-2	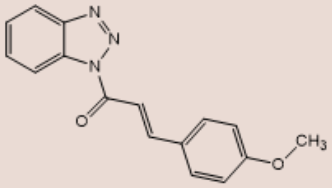	PT-8	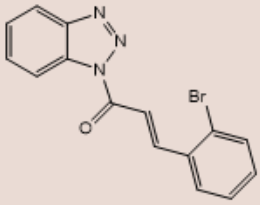
PT-3	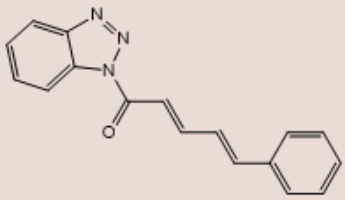	PT-9	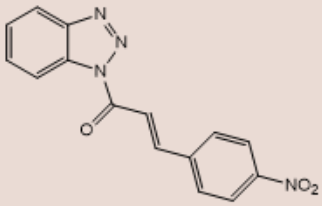
PT-4	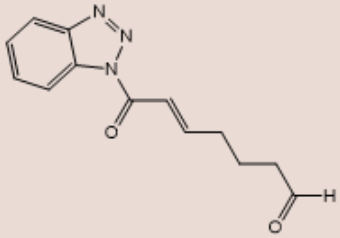	PT-10	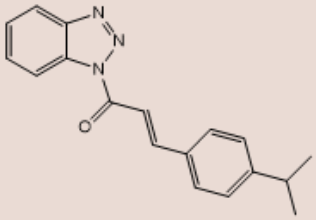
PT-5	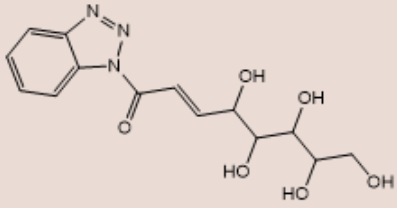	PT-11	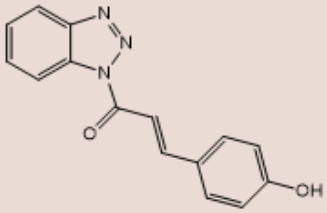
PT-6	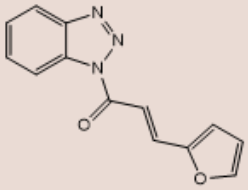	PT-12	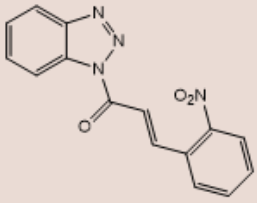

Table 2: Comparative Analysis of Physicochemical and Drug-Likeness Properties of PT-1 to PT-12.

Molecule	Rotable Bonds	HBA	HBD	Consensus Log P	Lipinski violation	Veber violation	Synthetic accessibility
PT-1	3	4	1	2.37	0	0	2.66
PT-2	4	4	0	2.81	0	0	2.62
PT-3	4	3	0	3.31	0	0	2.88
PT-4	6	4	0	1.95	0	0	2.55
PT-5	7	8	5	-0.88	0	1	4.14
PT-6	3	4	0	2.12	0	0	2.68
PT-7	4	5	2	O.54	0	0	3.04
PT-8	3	3	0	3.42	0	0	2.69
PT-9	4	5	0	2.05	0	0	2.62
PT-10	4	3	0	3.75	0	0	2.79
PT-11	3	4	1	2.4	0	0	2.57
PT-12	4	5	0	1.99	0	0	2.81

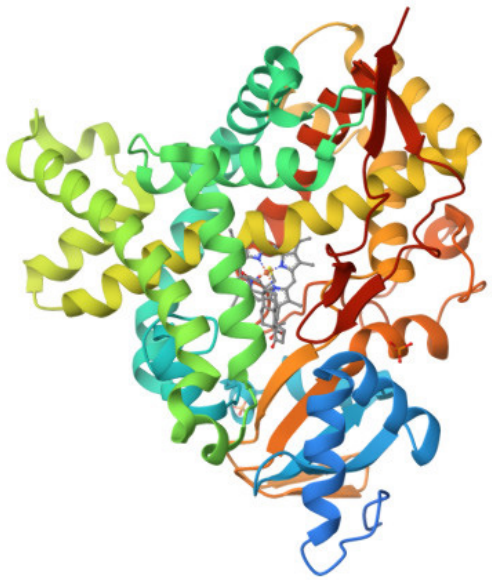

Figure 1: Crystal structure of human placental aromatase cytochrome P450 in complex with androstenedione of 3EQM | pdb_00003eqm.

evaluated CYP isoforms, indicating a more favorable metabolic safety profile. Importantly, none of the compounds inhibited CYP2D6 or CYP3A4, which are among the most clinically significant enzymes, thereby reducing the overall risk of severe drug–drug interactions. The skin permeation coefficient (Log Kp) values ranged from −5.09 to −9.64 cm/s, indicating generally low skin permeability across the series. Compounds such as PT-10, PT-3, and PT-8 demonstrated comparatively higher skin permeation potential (less negative Log Kp values), while PT-5 showed the lowest permeability, further corroborating its limited absorption profile. All compounds exhibited an identical bioavailability score of 0.55, suggesting moderate and consistent oral bioavailability potential throughout the series. This uniformity indicates that structural variations among the molecules did not significantly impact their predicted systemic availability. The comparative ADME analysis highlights PT-1, PT-4, PT-6, and PT-11 as particularly promising candidates due to their high GI absorption, BBB permeability, absence of major CYP inhibition, and favorable permeability characteristics. Conversely, PT-5 demonstrated comparatively suboptimal pharmacokinetic properties, including low GI absorption, lack of BBB permeability, and poor membrane permeation. The remaining compounds showed balanced ADME profiles but may require further optimization to minimize potential CYP-mediated drug.

Comparative Analysis of Drug-Likeness Parameters and Molecular Docking Scores of PT-1 to PT-12

The drug-likeness properties and binding affinities of the designed compounds (PT-1 to PT-12) were evaluated in Table 4; Figures 2 and 3 given the data of Comparison chart for Drug-Likeness Parameters and Molecular Docking based on Molecular Weight (MW), Hydrogen Bond Acceptors (HBA), Hydrogen Bond Donors (HBD), Lipophilicity (LogP), Polar Surface Area (PSA), and molecular docking scores against the target protein 3EQM. All compounds exhibited molecular weights below 500 Da, satisfying Lipinski's molecular weight criterion and indicating favorable oral drug-likeness. The number of hydrogen bond acceptors (3–8) and hydrogen bond donors (0–5) for most compounds remained within acceptable limits. However, PT-5, with 8 HBAs and 5 HBDs, approached the upper permissible threshold, suggesting increased polarity and hydrogen-bonding capacity. The LogP values ranged from 1.21 to 3.34, indicating moderate lipophilicity across the series. Compounds such as PT-2, PT-3, PT-8, and PT-10 demonstrated comparatively higher lipophilicity (LogP ≈ 3.0–3.34), which may favor membrane permeability, whereas PT-5 exhibited lower lipophilicity, consistent with its

elevated polar surface area. The Polar Surface Area (PSA) values varied significantly among the compounds, ranging from 47.78 to 148.93 Å². Most molecules showed PSA values below the recommended threshold of 140 Å², supporting good intestinal absorption. In contrast, PT-5 exceeded this limit (PSA = 148.93 Å²), which may adversely affect membrane permeability and oral bioavailability. Molecular docking studies against 3EQM revealed binding scores ranging from −6.22 to −9.90 kcal/mol, indicating favorable binding interactions for all compounds. Notably, PT-5 exhibited the strongest binding affinity (−9.90 kcal/mol), followed by PT-4 (−8.55 kcal/mol) and PT-11 (−7.26 kcal/mol), suggesting stable ligand–protein interactions. Despite its excellent docking score, the pharmacokinetic limitations of PT-5, particularly its high PSA and hydrogen bonding capacity, may restrict its *in vivo* applicability. Compounds such as PT-2, PT-3, PT-11, and PT-4 demonstrated a balanced profile, combining favorable docking scores with acceptable drug-likeness parameters. The comparative evaluation indicates that PT-4 and PT-11 emerge as promising lead candidates, exhibiting strong binding affinity toward 3EQM while maintaining compliance with Lipinski's criteria and favorable physicochemical properties. Although PT-5 showed superior docking performance, its reduced drug-likeness suggests that further structural optimization may be required to enhance its pharmacokinetic profile.

Binding interactions between the ligand and the active site residues of the target protein

The presented Table 5 containing diagram illustrates the binding interactions between the ligand and the active site residues of the target protein. The ligand is shown at the center in a ball-and-stick format, while the surrounding amino acid residues are represented as labeled nodes forming the binding pocket. Hydrogen bonds are indicated by green dashed lines, demonstrating strong and specific interactions between the ligand heteroatoms (such as N or O) and key amino acid residues. These interactions play a crucial role in ligand stabilization and binding specificity within the active site. Several surrounding residues contribute to hydrophobic contacts, shown by light green or gray shaded regions. These interactions enhance binding affinity by stabilizing the ligand through van der Waals forces and nonpolar contacts. Aromatic rings of the ligand participate in π–π stacking or π–alkyl interactions with aromatic or hydrophobic residues. These interactions are essential for anchoring the ligand inside the binding cavity and improving docking scores. Polar residues around the ligand contribute to electrostatic and dipole–dipole interactions, further strengthening ligand–protein association. The circular arrangement of residues indicates that the ligand is well-embedded within the active site cavity, suggesting good shape complementarity and favorable orientation for biological activity. The interaction map demonstrates that the ligand forms multiple stabilizing interactions, including hydrogen bonds and hydrophobic contacts, with critical amino acid residues of the target protein. This interaction profile supports the high docking score and predicted binding affinity, indicating that the ligand is a promising candidate for further biological evaluation.

DISCUSSION

The present study employed a structure-based molecular docking strategy to evaluate Benzotriazole derivatives as potential inhibitors of aromatase (CYP19A1), a validated target in hormone-dependent breast cancer. Aromatase catalyses the conversion of androgens into estrogens, and its overexpression in breast tissue contributes significantly to tumor progression in estrogen receptor–positive cancers (Mermer *et al.*, 2022). Targeting aromatase remains a clinically successful strategy; however, resistance and adverse effects associated with current inhibitors necessitate the discovery of novel scaffolds with improved efficacy and pharmacokinetic profiles (Noppawan *et*

Table 3: Comparative Analysis of Physicochemical and Drug-Likeness Properties of PT-1 to PT-12.

Molecule	Rotable Bonds	HBA	HBD	Consensus Log P	Lipinski violation	Veber violation	Synthetic accessibility
PT-1	3	4	1	2.37	0	0	2.66
PT-2	4	4	0	2.81	0	0	2.62
PT-3	4	3	0	3.31	0	0	2.88
PT-4	6	4	0	1.95	0	0	2.55
PT-5	7	8	5	-0.88	0	1	4.14
PT-6	3	4	0	2.12	0	0	2.68
PT-7	4	5	2	O.54	0	0	3.04
PT-8	3	3	0	3.42	0	0	2.69
PT-9	4	5	0	2.05	0	0	2.62
PT-10	4	3	0	3.75	0	0	2.79
PT-11	3	4	1	2.4	0	0	2.57
PT-12	4	5	0	1.99	0	0	2.81

al., 2025). Benzotriazole was selected as the core scaffold due to its nitrogen-rich heterocyclic structure, structural rigidity, and ability to participate in diverse non-covalent interactions (Omar *et al.*, 2022). The presence of multiple nitrogen atoms enhances hydrogen bonding capacity and electrostatic complementarity within protein active sites, while its aromatic system facilitates π–π stacking and hydrophobic interactions (Schneider *et al.*, 2011). These properties collectively contribute to strong ligand–protein binding affinity. Docking analysis against the crystal structure of aromatase (3EQM) demonstrated that all twelve compounds exhibited favorable binding energies ranging from −6.22 to −9.90 kcal/mol. Among them, PT-5 displayed the highest binding affinity (−9.90 kcal/mol), forming multiple conventional hydrogen bonds with VAL369, VAL370, PRO429, and MET311. The short bond distances (1.79–2.63 Å) indicate strong and stable interactions. Additionally, PT-5 engaged in

Table 4: Comparative Analysis of Drug-Likeness Parameters and Molecular Docking Scores of PT-1 to PT-12.

COM.	MW	HBA	HBD	Log P	TPSA	DOCKING SCORE
	<500	<10	<5	<5	<140	3EQM
PT-1	265.27	4	1	2.21	68.01	-6.87
PT-2	279.29	4	0	3.02	57.01	-7.13
PT-3	275.3	3	0	3.02	47.78	-7.00
PT-4	243.26	4	0	2.23	64.85	-8.55
PT-5	323.3	8	5	1.21	148.93	-9.90
PT-6	239.23	4	0	2.5	60.92	-6.35
PT-7	233.22	5	2	1.86	88.24	-6.22
PT-8	328.16	3	0	3	47.78	-6.80
PT-9	294.26	5	0	2.33	93.6	-6.71
PT-10	291.35	3	0	3.34	47.78	-6.66
PT-11	265.27	4	1	2.35	68.01	-7.26
PT-12	294.26	5	0	2.03	93.6	-6.65

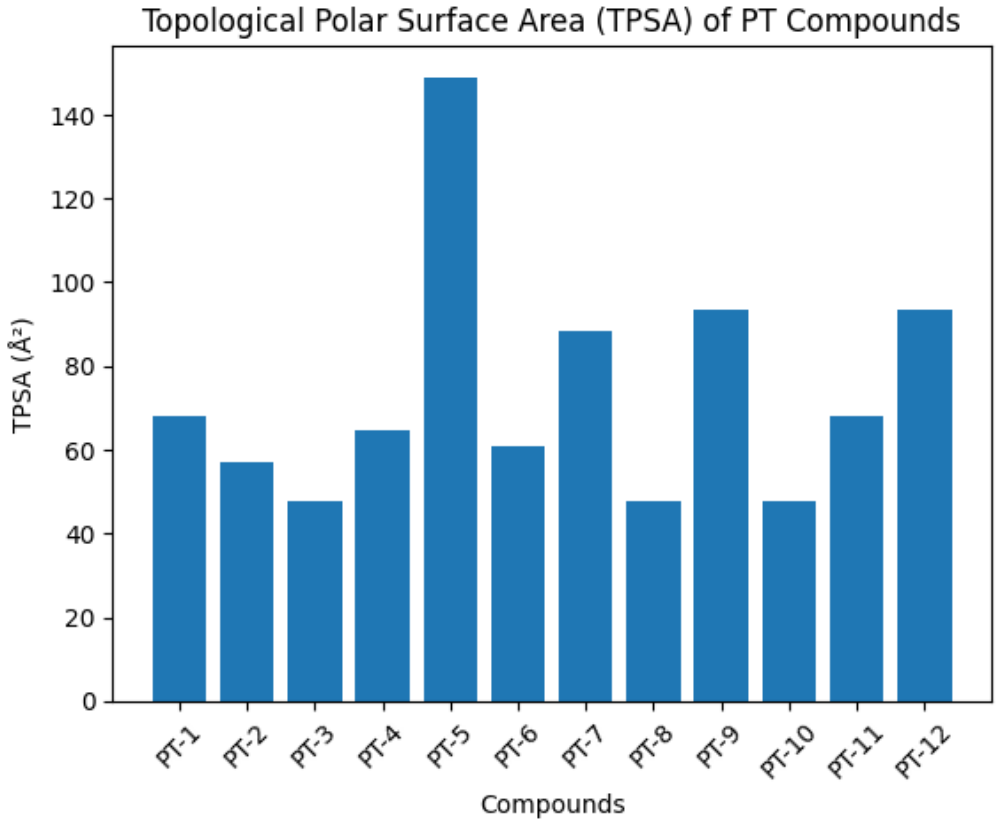

Figure 2: Comparison chart for TPSA data for Benzotriazole Derivatives from PT-1 to PT-12.

Table 5: Comparative Analysis of 2D Interaction and 3D Interaction with different Amino acids.

Name	2D Interaction	3D Interactions
PT-1		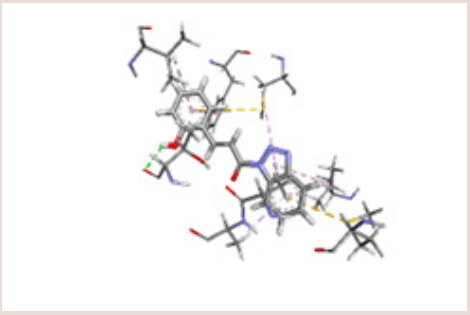
PT-2		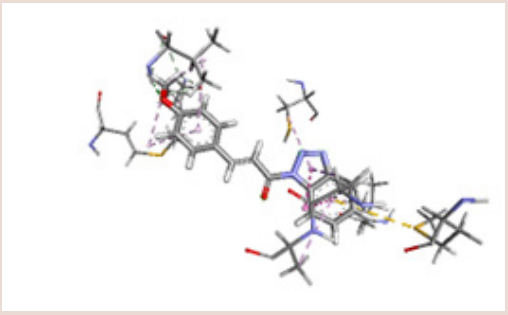
PT-3		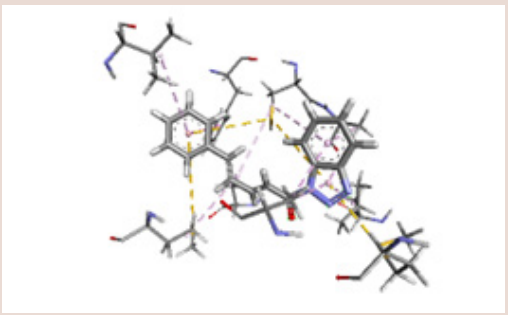
PT-4		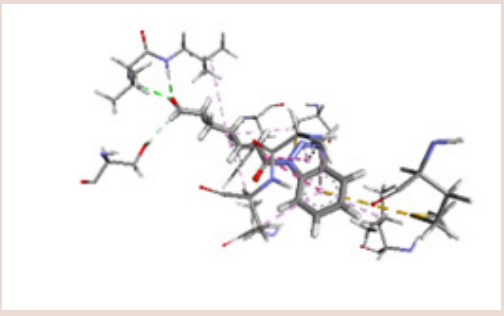

Name	2D Interaction	3D Interactions
PT-5		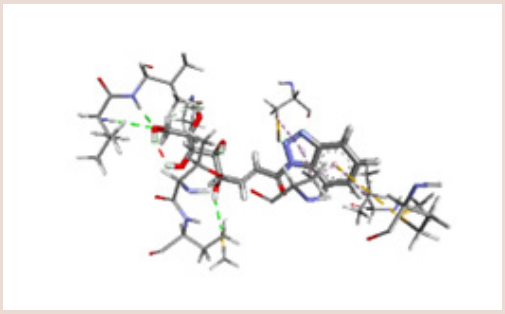
PT-6		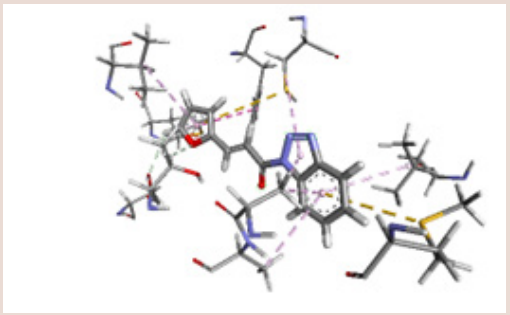
PT-7		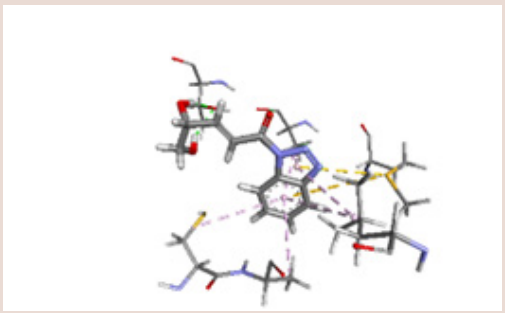
PT-8		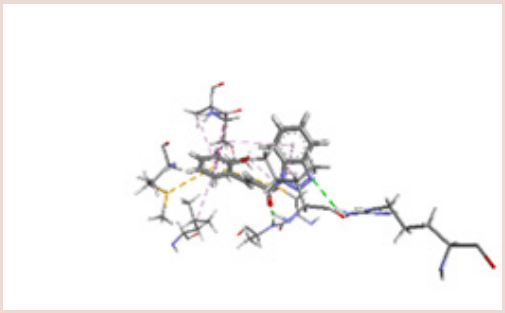

Name	2D Interaction	3D Interactions
PT-9		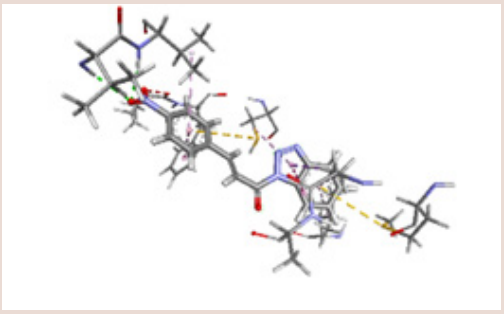
PT-10		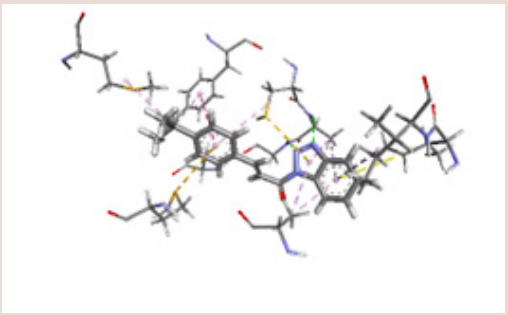
PT-11	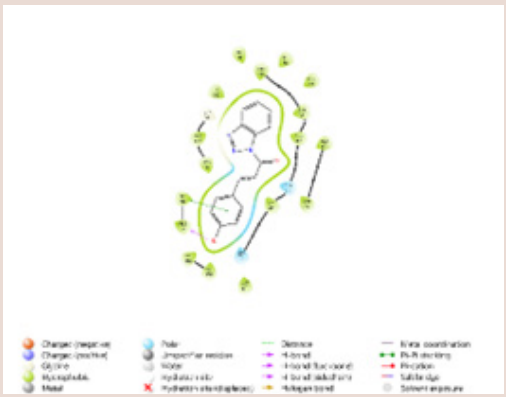	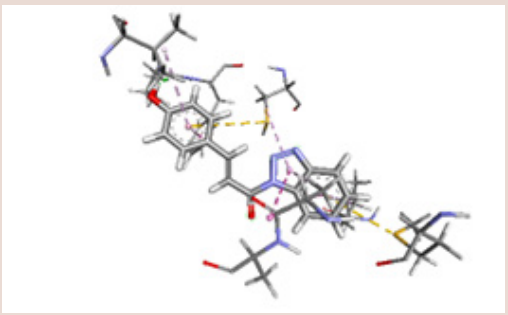
PT-12		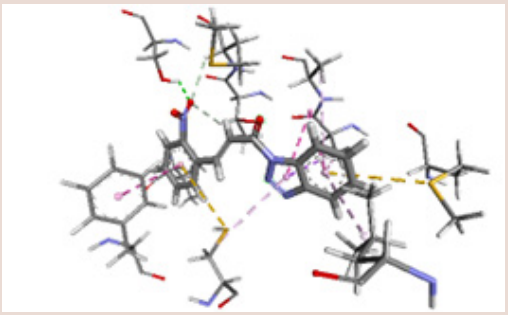

π–sulfur interactions with MET303 and hydrophobic contacts with ALA306 and LEU152, reinforcing ligand stabilization within the active site cavity. PT-4 and PT-11 emerged as particularly promising candidates due to their balanced interaction profiles. PT-4 formed strong hydrogen bonds with VAL369 and VAL370 along with amide–π stacking interactions involving ALA306 and ALA307. PT-11 demonstrated a stable hydrogen bond with PRO429 and significant π–π stacking interactions with PHE430. These residues—VAL369, VAL370, ALA306, ALA307, LEU152, PHE430, MET303, and CYS437—collectively constitute the core binding environment of the aromatase active site and were consistently involved across multiple ligand complexes. Although PT-5 showed superior docking performance, its high polar surface area (148.93 Å^2), increased hydrogen bond donors and acceptors, and Veber rule violation suggest potential limitations in membrane permeability and oral bioavailability. Conversely, PT-4 and PT-11 demonstrated optimal physicochemical parameters, including molecular weights below 500 Da, LogP values within acceptable limits, and compliance with both Lipinski and Veber criteria (Sleightholm *et al.*, 2021). These findings indicate that PT-4 and PT-11 possess a more favorable balance between binding affinity and drug-likeness. ADME analysis further supported these observations. Most compounds exhibited high gastrointestinal absorption and acceptable bioavailability scores (0.55). Notably, PT-1, PT-4, PT-6, and PT-11 displayed minimal cytochrome P450 inhibition, suggesting lower risk of metabolic drug–drug interactions. In contrast, PT-2, PT-3, PT-8, and PT-10 showed predicted inhibition of certain CYP isoforms, which may require structural refinement to reduce metabolic liabilities (Soragni *et al.*, 2025). The interaction patterns observed—hydrogen bonding, π–π stacking, π–alkyl, and π–sulfur contacts—highlight the importance of aromatic and hydrophobic complementarity within the aromatase binding pocket. The benzotriazole scaffold effectively anchors within the cavity while allowing functional group modifications that influence polarity, lipophilicity, and binding strength. Structure–activity insights suggest that moderate lipophilicity and controlled hydrogen bonding capacity are essential for maintaining both strong docking performance and favorable pharmacokinetic characteristics. The binding modes of the designed compounds (PT-1 to PT-12) within the active site of the target protein (3EQM) were analyzed based on hydrogen bonding, hydrophobic contacts, and other non-covalent interactions, including π–π, π–alkyl, π–sulfur, and amide–π stacking interactions. These interactions collectively contribute to ligand stabilization and binding affinity. Hydrogen bond formation was observed in most compounds, indicating favorable anchoring within the binding pocket. PT-4 and PT-5 exhibited the highest number of strong conventional hydrogen bonds, particularly with key residues VAL369, VAL370, PRO429, MET311, and THR310, with bond distances ranging from 1.79 to 2.63 Å (Table 6), suggesting highly stable ligand–protein interactions. PT-2 and PT-9 also formed multiple hydrogen bonds with VAL370, highlighting the importance of this residue in ligand recognition. In contrast, PT-3 showed no hydrogen bonding interactions, relying predominantly on hydrophobic and π-mediated contacts for binding stabilization. Hydrophobic interactions were dominant across all complexes, involving residues such as ALA306, ALA307, LEU152, VAL370, PHE430,

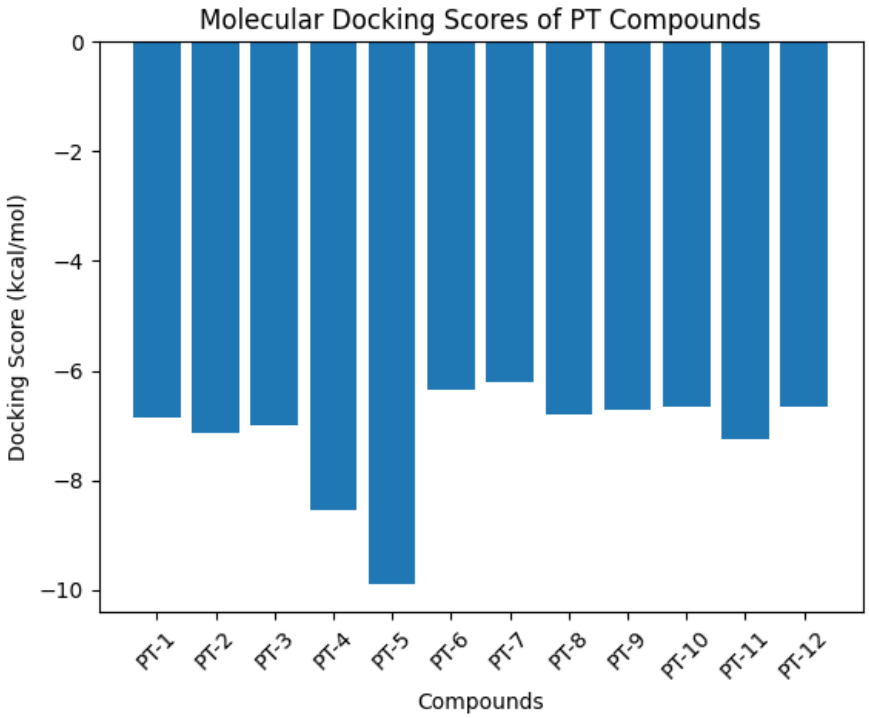

Figure 3: Comparative Analysis of Molecular Docking Scores of PT-1 to PT-12.

CYS437, and MET364. These residues consistently participated in π–alkyl, alkyl, and π–π T-shaped interactions, forming a hydrophobic core that supports ligand accommodation. PT-1, PT-6, PT-7, and PT-11 exhibited extensive π–alkyl interactions with ALA306 and LEU152, indicating strong van der Waals stabilization. Aromatic stacking interactions were evident in several complexes. PHE430 contributed to π–π T-shaped interactions in PT-1, PT-3, PT-6, PT-9, PT-10, PT-11, and PT-12, underscoring its role in reinforcing ligand orientation within the binding cavity. Additionally, amide–π stacking interactions involving ALA306 and ALA307 were frequently observed in PT-2, PT-4, PT-8, PT-9, PT-11, and PT-12, further enhancing binding stability. π–sulfur interactions were commonly detected with sulfur-containing residues MET303, MET311, and CYS437, particularly in PT-3, PT-4, PT-6, PT-8, PT-9, PT-10, and PT-12. These interactions contributed additional stabilization through favorable sulfur–aromatic contacts. The frequent involvement of MET303 suggests its critical role in ligand binding across the compound series. Among the studied compounds, PT-5 demonstrated the most diverse interaction profile, forming multiple conventional and carbon hydrogen bonds alongside extensive hydrophobic and π-interactions, which correlates well with its superior docking score. PT-4 and PT-11 also displayed balanced interaction patterns, combining strong hydrogen bonding with dense hydrophobic networks, supporting their favorable binding affinities given in Table 5. Compounds such as PT-3 and PT-7, despite fewer hydrogen bonds, maintained stable binding through extensive hydrophobic and π-mediated

Table 6: Comparative Analysis of Name amino acids with their Distance and its Category of PT1-PT12 derivatives.

Name	Distance	Category	Name	Distance	Category
PT-1			**PT-7**		
THR310	2.96882	Hydrogen Bond	THR310	2.18729	Hydrogen Bond
MET303	4.4833	Other	THR310	2.02948	Hydrogen Bond
CYS437	5.41865	Other	MET303	5.67846	Other
PHE430	4.99318	Hydrophobic	MET303	4.78284	Other
LEU152	4.80267	Hydrophobic	LEU152	5.35403	Hydrophobic
ALA306	3.5599	Hydrophobic	ALA306	3.80297	Hydrophobic
ALA307	4.59799	Hydrophobic	CYS437	5.29547	Hydrophobic
LEU152	5.43815	Hydrophobic	ALA438	4.42862	Hydrophobic
ALA306	3.72951	Hydrophobic	LEU152	4.62243	Hydrophobic
CYS437	5.2582	Hydrophobic	ALA306	3.47152	Hydrophobic
VAL370	4.3562	Hydrophobic			
PT-2			**PT-8**		
VAL370	2.24913	Hydrogen Bond	ARG115	2.92315	Hydrogen Bond
VAL370	2.59049	Hydrogen Bond	ALA438	2.01391	Hydrogen Bond
VAL370	2.42812	Hydrogen Bond	MET303	4.84547	Other
PRO429	2.49137	Hydrogen Bond	CYS437	5.94868	Other
PRO429	2.4773	Hydrogen Bond	ALA306,	4.64801	Hydrophobic
ALA306	2.84276	Hydrophobic	ALA443	4.2351	Hydrophobic
MET303	4.99651	Other	CYS437	4.59717	Hydrophobic
ALA306,	4.58449	Hydrophobic	ILE133	4.31492	Hydrophobic
ALA306,	4.69101	Hydrophobic	ALA306	5.21102	Hydrophobic
MET364	4.66692	Hydrophobic	ILE133	4.17725	Hydrophobic
VAL370	4.15192	Hydrophobic	LEU152	4.77103	Hydrophobic
PRO429	5.48796	Hydrophobic	ALA306	3.65644	Hydrophobic
LEU152	4.86962	Hydrophobic	ALA307	4.83003	Hydrophobic
ALA306	3.56519	Hydrophobic			
ALA307	4.92144	Hydrophobic			
CYS437	4.76704	Hydrophobic			
MET364	5.0182	Hydrophobic			

Name	Distance	Category	Name	Distance	Category
VAL370	4.30079	Hydrophobic			
PT-3			**PT-9**		
MET303	4.19692	Other	VAL369	2.32035	Hydrogen Bond
MET311	5.63322	Other	VAL370	2.03455	Hydrogen Bond
CYS437	5.90244	Other	ALA306	2.69071	Hydrophobic
CYS437	5.28584	Other	MET303	4.70707	Other
PHE430	5.10783	Hydrophobic	CYS437	5.49109	Other
CYS437	5.1332	Hydrophobic	PHE430	5.08784	Hydrophobic
ALA443	3.66221	Hydrophobic	ALA306	4.74425	Hydrophobic
MET311	4.75782	Hydrophobic	LEU152	4.62361	Hydrophobic
ALA306	4.21791	Hydrophobic	ALA306	3.39379	Hydrophobic
CYS437	5.41512	Hydrophobic	CYS437	4.6665	Hydrophobic
ALA438	4.1033	Hydrophobic	VAL370	4.45271	Hydrophobic
LEU152	4.57364	Hydrophobic			
ALA306	3.45189	Hydrophobic			
ALA438	4.9898	Hydrophobic			
VAL370	5.03991	Hydrophobic			
PT-4			**PT-10**		
VAL369	2.21648	Hydrogen Bond	ALA438	2.60867	Hydrogen Bond
VAL370	2.01711	Hydrogen Bond	GLY439	2.39307	Hydrogen Bond
SER314	2.68875	Hydrogen Bond	MET311	4.67425	Other
MET303	4.83968	Other	CYS437	4.43411	Other
ALA306,	4.6202	Hydrophobic	PHE430	5.60837	Hydrophobic
ALA306,	4.71078	Hydrophobic	MET364	4.87052	Hydrophobic
VAL370	5.08303	Hydrophobic	PHE430	5.1039	Hydrophobic
CYS437	5.21565	Hydrophobic	CYS437	4.95118	Hydrophobic
ALA443	5.37644	Hydrophobic	ALA443	4.40424	Hydrophobic
PHE430	4.98588	Hydrophobic	ILE132	5.46987	Hydrophobic
LEU152	4.79833	Hydrophobic	ILE133	5.06299	Hydrophobic
ALA306	3.67739	Hydrophobic	ALA306	3.96077	Hydrophobic
ALA307	4.73844	Hydrophobic	ALA438	4.90295	Hydrophobic
ALA306	3.75084	Hydrophobic	ALA306	4.27548	Hydrophobic
CYS437	4.98458	Hydrophobic	ALA438	4.04656	Hydrophobic
PT-5			**PT-11**		
VAL369	2.63017	Hydrogen Bond	PRO429	2.08544	Hydrogen Bond
VAL370	1.79006	Hydrogen Bond	MET303	4.46377	Other
PRO429	2.04461	Hydrogen Bond	CYS437	5.01729	Other
MET311	2.47151	Hydrogen Bond	PHE430	4.91534	Hydrophobic
THR310	2.53638	Hydrogen Bond	ALA306	4.93934	Hydrophobic
PRO429	2.96785	Hydrogen Bond	ALA306	4.72297	Hydrophobic
MET303	4.61263	Other	LEU152	4.57594	Hydrophobic
ALA306	3.60766	Hydrophobic	ALA306	3.34433	Hydrophobic
CYS437	4.66655	Hydrophobic	ALA306	3.81732	Hydrophobic

Name	Distance	Category	Name	Distance	Category
LEU152	4.79579	Hydrophobic	CYS437	4.8648	Hydrophobic
ALA306	3.37631	Hydrophobic	VAL370	4.59262	Hydrophobic
PT-6			**PT-12**		
THR310	2.69198	Hydrogen Bond	SER314	2.61698	Hydrogen Bond
SER314	2.90424	Hydrogen Bond	THR310	2.71282	Hydrogen Bond
MET303	4.61374	Other	MET311	2.6614	Hydrogen Bond
CYS437	5.7599	Other	ALA306	2.67973	Hydrophobic
PHE430	5.25436	Hydrophobic	MET303	4.60521	Other
ALA306	3.88171	Hydrophobic	CYS43	5.04348	Other
CYS437	5.07212	Hydrophobic	PHE430	4.8468	Hydrophobic
LEU152	4.83987	Hydrophobic	ALA306	4.82997	Hydrophobic
ALA306	3.5072	Hydrophobic	ALA306	4.57521	Hydrophobic
ALA307	4.66204	Hydrophobic	LEU152	4.63139	Hydrophobic
MET364	5.45853	Hydrophobic	ALA306	3.4018	Hydrophobic
VAL370	4.57771	Hydrophobic	ALA307	5.38782	Hydrophobic

interactions. The comparative interaction analysis reveals that residues VAL369, VAL370, ALA306, ALA307, LEU152, PHE430, MET303, and CYS437 constitute the core binding environment of the 3EQM active site. Overall, this *in silico* investigation demonstrates that Benzotriazole derivatives, particularly PT-4 and PT-11, represent promising lead candidates for aromatase inhibition. While PT-5 showed the strongest theoretical binding, its pharmacokinetic limitations highlight the importance of balancing affinity with drug-like properties. Further validation through molecular dynamics simulations, enzyme inhibition assays, and *in vitro* anticancer studies is necessary to confirm the therapeutic potential of these compounds. The present findings provide a rational framework for the continued optimization of Benzotriazole-based aromatase inhibitors in breast cancer drug discovery.

CONCLUSION

The present study employed a comprehensive structure-based molecular docking approach to evaluate benzotriazole derivatives as potential aromatase (CYP19A1) inhibitors for hormone-dependent breast cancer therapy. The designed benzotriazole derivatives (PT-1 to PT-12) demonstrated favorable binding affinities toward the active site of aromatase (PDB ID: 3EQM), with docking scores ranging from −6.22 to −9.90 kcal/mol. Among the series, PT-5 exhibited the strongest theoretical binding affinity, forming multiple conventional hydrogen bonds and extensive hydrophobic and π-mediated interactions with key active-site residues such as VAL369, VAL370, PRO429, MET303, MET311, ALA306, LEU152, PHE430, and CYS437. These interactions contributed significantly to ligand stabilization within the binding cavity. Despite its superior docking score, PT-5 showed comparatively higher polarity and one Veber rule violation, which may limit its membrane permeability and oral bioavailability. In contrast, PT-4 and PT-11 emerged as the most promising lead candidates due to their balanced profiles, combining strong binding interactions with favorable physicochemical properties. Overall, the findings highlight the benzotriazole scaffold as a promising structural framework for the development of novel aromatase inhibitors. The integration of molecular docking, drug-likeness evaluation, and ADME prediction provides a rational basis for lead optimization. Further validation through molecular dynamics simulations, enzymatic inhibition assays, and *in vitro* and *in vivo* anticancer studies is warranted to confirm the therapeutic potential of the identified lead compounds.

ACKNOWLEDGEMENT

The authors are Thankful to Pravara Rural College of Pharmacy, Pravaranagar.

ABBREVIATIONS

ADME: Absorption, Distribution, Metabolism, and Excretion; **BBB:** Blood–Brain Barrier; **CNS:** Central Nervous System; **CYP:** Cytochrome P450; **CYP1A2:** Cytochrome P450 1A2; **CYP2C19:** Cytochrome P450 2C19; **CYP2C9:** Cytochrome P450 2C9; **CYP2D6:** Cytochrome P450 2D6; **CYP3A4:** Cytochrome P450 3A4; **GI:** Gastrointestinal; **HBA:** Hydrogen Bond Acceptor; **HBD:** Hydrogen Bond Donor; **Log Kp:** Logarithm of Skin Permeation Coefficient; **LogP:** Logarithm of Octanol: Water Partition Coefficient; **MW:** Molecular Weight; **PSA:** Polar Surface Area; **PT:** Designed Benzotriazole / Proposed Test Compound (PT-1 to PT-12); **SA Score:** Synthetic Accessibility Score.

CONFLICT OF INTEREST

The authors declare that there is no conflict of interest.

REFERENCES

Agu, P. C., Afiukwa, C. A., Orji, O. U., *et al*. (2023). Molecular docking as a tool in drug discovery. *Scientific Reports, 13*, 13398. https://doi.org/10.1038/s41598-023-40521-9

Arvindekar, S. A., Rathod, S., Choudhari, P. B., et al. (2024). Computational discovery of aromatase modulators. *BioImpacts, 14*(5), 277–283. https://doi.org/10.34172/bi.2024.277

Augusto, T. V., Correia-da-Silva, G., Rodrigues, C. M. P., Teixeira, N., & Amaral, C. (2018). Acquired resistance to aromatase inhibitors. *Endocrine-Related Cancer, 25*(5), R283–R301. https://doi.org/10.1530/ERC-17-0449

Bhatia, N., & Thareja, S. (2025). 3D-QSAR and docking studies on aromatase inhibitors. *Letters in Drug Design & Discovery, 22*(1), 100007. https://doi.org/10.2174/1570180822666250107100007

Briguglio, I., Piras, S., Corona, P., *et al*. (2015). Benzotriazole: Versatile biological behavior. *European Journal of Medicinal Chemistry, 97*, 612–648. https://doi.org/10.1016/j.ejmech.2014.10.014

Du, X., Li, Y., Xia, Y. L., *et al*. (2016). Insights into protein–ligand interactions: Mechanisms, models, and methods. *International Journal of Molecular Sciences, 17*(2), 144. https://doi.org/10.3390/ijms17020144

Eissa, M. A., & Gohar, E. Y. (2023). Aromatase enzyme: Paving the way for exploring aromatization for cardio-renal protection. *Biomedicine & Pharmacotherapy, 168*, 115832. https://doi.org/10.1016/j.biopha.2023.115832

Freihat, O., Sipos, D., & Kovacs, A. (2025). Global burden and projections of breast cancer incidence and mortality to 2050. *Frontiers in Public Health, 13*, 1622954. https://doi.org/10.3389/fpubh.2025.1622954

Gadakh, S., Aghav, B., Teraiya, N., *et al*. (2025). Discovery of novel benzoxazole analogues targeting aromatase. *Bioorganic & Medicinal Chemistry, 122*, 118142. https://doi.org/10.1016/j.bmc.2025.118142

Gumede, N. J., Bisetty, K., Escuder-Gilabert, L., *et al*. (2025). Evaluation of CYP19A1-mediated aromatase inhibitors. *Results in Chemistry, 16*, 102355. https://doi.org/10.1016/j.rechem.2025.102355

Kifle, Z. D., Tadele, M., Alemu, E., Gedamu, T., & Ayele, A. G. (2021). Recent development of new therapeutic agents and novel drug targets for cancer treatment. *SAGE Open Medicine, 9*, 20503121211067083. https://doi.org/10.1177/20503121211067083

Lee, H., Hurh, S., Kang, S., et al. (2025). Identification of chemical scaffolds via virtual screening. *Journal of Enzyme Inhibition and Medicinal Chemistry, 40*(1), 2518191. https://doi.org/10.1080/14756366.2025.2518191

Lewis-Wambi, J. S., & Jordan, V. C. (2009). Estrogen regulation of apoptosis. *Breast Cancer Research, 11*(3), 206. https://doi.org/10.1186/bcr2255

Li, X., Zhang, Y., Wang, L., & Chen, J. (2020). Synthesis and anticancer activity of benzotriazole derivatives. *Journal of Heterocyclic Chemistry, 57*(10), 3812–3820. https://doi.org/10.1002/jhet.3859

Ma, X., & Yu, H. (2006). Global burden of cancer. *Yale Journal of Biology and Medicine, 79*(3–4), 85–94. https://doi.org/10.1002/ydm.2006.79.issue-3-4

Mardale, G., Prodea, A., Munteanu, A., *et al*. (2026). Benzotriazole in cancer: A systematic review. *Pharmaceuticals, 19*(1), 77. https://doi.org/10.3390/ph19010077

Mermer, A., Bulbul, M. V., Kalender, S. M., *et al*. (2022). Benzotriazole-oxadiazole hybrid compounds. *Journal of Molecular Liquids, 359*, 119264. https://doi.org/10.1016/j.molliq.2022.119264

Noppawan, P., Worawut, K., Kunnasut, S., *et al*. (2025). Benzotriazole derivatives: Versatile scaffolds in medicinal chemistry. *Chimica Techno Acta, 12*. https://doi.org/10.15826/chimtech.2025.12.4

Omar, A. M., Aljahdali, A. S., Safo, M. K., *et al*. (2022). Docking and molecular dynamic investigations. *Molecules, 28*(1), 44. https://doi.org/10.3390/molecules28010044

Schneider, R., Barakat, A., Pippen, J., & Osborne, C. (2011). Aromatase inhibitors in breast cancer treatment. *Breast Cancer: Targets and Therapy, 3*, 113–125. https://doi.org/10.2147/BCTT.S17726

Sleightholm, R., Neilsen, B. K., Elkhatib, S., *et al*. (2021). Percentage of hormone receptor positivity in breast cancer provides prognostic value. *Journal of Clinical Medicine Research, 13*(1), 9–19. https://doi.org/10.14740/jocmr4404

Soragni, A., Knudsen, E. S., O'Connor, T. N., *et al*. (2025). Acquired resistance in cancer: Towards targeted therapeutic strategies. *Nature Reviews Cancer, 25*(8), 613–633. https://doi.org/10.1038/s41568-025-00600-0

Cite this article: Tambe PR, Bhor RJ, Kolhe MH, Varade RB, Bhaiya ST, Tambe AS. Benzotriazole as Privileged Scaffold: A Molecular Docking Approach toward Breast Cancer Drug Discovery. Asian J Biol Life Sci. 2026;15(1):159-72.